

Competition between initial- and final-state effects in valence- and core-level x-ray photoemission of Sb-doped SnO_2

R. G. Egdell,* J. Rebane,[†] and T. J. Walker

Inorganic Chemistry Laboratory, South Parks Road, Oxford OX1 3QR, United Kingdom

D. S. L. Law

Research Unit for Surfaces Transforms and Interfaces, Daresbury Laboratory, Warrington, Cheshire WA4 4AD, United Kingdom

(Received 20 July 1998)

High resolution valence- and core-level photoemission spectra of undoped and 3% Sb-doped SnO_2 are presented. Conduction-band occupation due to Sb doping in SnO_2 leads to a shift of valence-band features to high binding energy. However, the shift is less than the width of the occupied part of the conduction band. This is attributed to a shrinkage of the bulk band gap with doping, arising from an attractive dopant electron interaction and screening of the Coulomb repulsion between valence and conduction electrons. Core-level spectra provide evidence for strong screening by the conduction electron gas in 3% Sb-doped SnO_2 , giving rise to “screened” and “unscreened” final-state peaks in photoemission. The dominant screening response involves excitation of conduction electron plasmons. [S0163-1829(99)04803-1]

I. INTRODUCTION

The oxide SnO_2 adopts the tetragonal rutile structure and has a direct (but dipole forbidden) band gap of 3.62 eV.¹ The solid is amenable to n -type doping to produce a material that combines high conductivity with transparency in the visible region. The optical “window” is limited at low energy by the onset of a high reflectivity below the conduction electron plasmon frequency; and at high energy by excitation from valence-band states into empty conduction-band states. The remarkable conjunction of physical properties leads to exploitation of doped SnO_2 in a variety of applications including transparent conducting (and therefore heatable) windows, heat reflecting double glazing, as well as in more sophisticated devices including solar cells, liquid crystal displays, etc.²

Most previous work on the effects of doping on the electronic properties of post-transition metal-oxide semiconductors has focused on trying to understand changes in electronic absorption spectra induced by doping. In particular, Berggren and Sernelius have developed a general approach to calculation of band-gap shifts in doped semiconductors.³ This has been applied to rationalize shifts in optical absorption onsets with doping in ZnO ,⁴ In_2O_3 ,⁵ and SnO_2 .⁶ The main features of this model when applied to a direct gap semiconductor with upward conduction-band dispersion and downward valence-band dispersion away from the Γ point are as follows. In undoped material, the absorption onset corresponds to promotion of valence electrons from the top of the valence band at Γ to the bottom of the conduction band, also at Γ . Above the Mott critical density n -type doping blocks the states at the bottom of the conduction band up to a wave vector k_F and therefore causes the lowest-energy transitions to originate from valence-band states at $k=k_F$. The band-gap widening thus caused is called the Burstein-Moss shift⁷ and depends on both the upward conduction-band dispersion and downward valence-band dispersion. Be-

cause the conduction-band effective mass is usually less than the valence-band effective mass, the conduction-band dispersion dominates overall shift. However at the same time the doping is associated with electron-dopant interactions and the conduction electron gas screens the Coulomb repulsion between valence and conduction electrons. These effects lead to a shrinkage or renormalization of the host band gap, reducing the magnitude of the Burstein-Moss shift.

We have recently shown that by studying shifts in valence region photoemission spectra of doped CdO in relation to the width of the occupied part of the conduction band it is possible to obtain a direct measurement of band-gap shrinkage.⁸ In the present paper we extend this approach to study the effects of Sb doping in SnO_2 . However, the main focus of the paper is on the effects of doping on core level spectra. In the simplest rigid band model, doping should produce a shift in core-level binding energies that mirrors the changes found in the valence region. However, the issue of whether the rigid band model is applicable to understanding shifts in core levels of doped oxides has aroused much controversy since the early 1980's, when conflicting experimental evidence emerged regarding the influence of Na doping on core binding energies in Na_xWO_3 .⁹⁻¹¹ More recent interest in this area has derived from the study of the effects of p - and n -type doping in superconducting cuprates.¹²⁻¹⁴

II. EXPERIMENT

High purity tin(IV) oxide was obtained from Johnson Matthey. Phase pure 3% antimony-doped tin oxide was prepared by a coprecipitation procedure, as described previously.¹⁵⁻¹⁷ The powders were pressed into 13-mm pellets and sintered in air at 1000 °C for several days to yield strong ceramic disks.

Preliminary x-ray photoemission spectra and electron energy loss spectra were measured in an ESCALAB spectrom-

eter (VG Scientific) equipped with a twin anode x-ray source and low-energy electron gun. The mode of operation of this spectrometer and its application to the study of electron spectra of SnO_2 has been described in detail elsewhere.^{15–17}

High-resolution x-ray photoemission spectra were measured in a Scienta ESCA 300 spectrometer. This incorporates a rotating anode x-ray source, a seven-crystal x-ray monochromator and a 300-mm mean radius spherical sector electron energy analyser with parallel electron detection system. The x-ray source was run with 200 mA emission current and 14 kV anode bias, whilst the analyser operated at 150 eV pass energy with 0.5-mm slits. Gaussian convolution of the analyzer resolution with a linewidth of 260 meV for the x-ray source gives an effective instrument resolution of 350 meV. Binding energies are referenced to the Fermi energy of an ion bombarded silver foil that is regularly used to calibrate the spectrometer.

The ceramic pellets of undoped SnO_2 and 3% Sb-doped SnO_2 were cleaned *in situ* in the preparation chamber of the Scienta spectrometer by annealing in UHV at about 750 °C for 2–3 h, heating being effected by an electron beam heater. Surfaces prepared in this way were free of structure due to carbon or other contaminants and remained clean for the duration of the spectroscopic measurements.

Binding energies are referenced to the Fermi energy of a silver foil regularly used to calibrate the spectrometer. There was no indication of sample charging during the x-ray photoemission spectroscopy (XPS) measurements.

III. RESULTS AND DISCUSSION

A. Valence-band photoemission

Valence-band photoemission spectra of nominally undoped SnO_2 and 3% Sb-doped SnO_2 are shown in Fig. 1. The spectra display a characteristic three-peaked structure consistent with previous XPS data.^{18–20} In addition, the spectrum of undoped SnO_2 shows a weak but well-defined shoulder on the low binding energy side that tails into the bulk band gap. This latter feature is also observed in photoemission from ordered $\text{SnO}_2(110)$ surfaces from which bridging oxygen ions that are normally present on the stoichiometric surface have been removed.^{21–24} This brings about reduction of half the surface Sn ions from Sn(IV) to Sn(II). Electric field gradients at the surface site induce mixing between Sn 5s and Sn 5p states, and a 5s-5p hybrid state is pushed down toward the bottom of the bulk band gap.^{24,25} The gap peak on the present polycrystalline surface must have a similar origin: in view of the physical mechanisms responsible, Sn(II) surface states toward the bottom of the bulk band gap are expected to arise at all SnO_2 surfaces that become oxygen deficient. The gap shoulder is much less pronounced for 3% Sb-doped SnO_2 , although there is still weak tailing into the gap. This attributed to segregation of Sb(III) ions to surface sites where they replace Sn(II) cations. The Sb(III) surface state must lie at lower energy than the corresponding Sn(II) surface state, so that the spectral feature now overlaps the valence band more strongly. The segregation model is supported by the observation that Sb core-level peaks are much more intense than expected from the bulk doping level (see below).

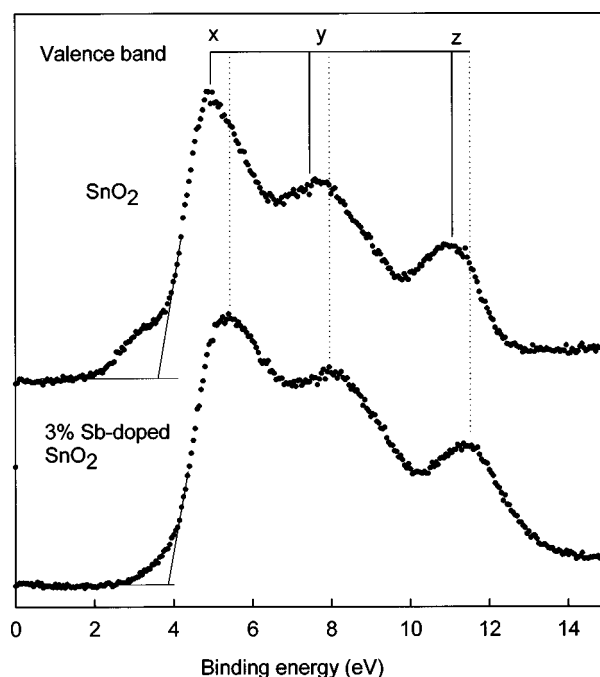


FIG. 1. Valence-band XPS of undoped SnO_2 and 3% Sb-doped SnO_2 . Linear extrapolations of the valence-band edges are shown: these allow estimates to be made of the valence-band onset energies. Vertical lines highlight shifts in the valence band peaks x, y, and z with doping. The peak positions were determined by fitting the valence-band profile to a series of Voigt peaks. See text for details.

Due to the presence of the band-gap peak in undoped SnO_2 , it is a little difficult to locate the exact position of the valence-band onset. However, a simple linear extrapolation procedure places the onset at about 3.60 ± 0.05 eV binding energy relative to the Fermi level. This accords with the quoted bulk band gap of 3.62 eV for SnO_2 and the pinning of the Fermi level very close to the bottom of the Sn 5s conduction band by donor states induced by oxygen deficiency. The valence-band onset as defined by the linear extrapolation of the valence-band edge shows a shift to 3.95 ± 0.05 eV upon Sb doping. The 0.35-eV shift is attributed to occupation of conduction-band states in degenerately doped SnO_2 . Shifts in the valence-band peaks are also found and are given in Table I. The binding energies here were defined by fitting the valence-band spectra to a set of three Voigt peaks, with an additional peak for the gap state. The mean shift in the valence band features is 0.45 eV.

It is interesting to evaluate the magnitude of the shift in relation to the width of the occupied part of the Sn 5s conduction band. The low concentration of charge carriers coupled with the very low cross section for ionization of Sn 5 states at x-ray photon energy precludes direct observation of conduction-band features in the present experiment. However, we can estimate the expected bandwidth using a procedure based on measurement of the energy of the surface plasmon in low-energy electron energy-loss spectroscopy (EELS).⁸

The conduction electrons in doped SnO_2 gives rise to a characteristic plasmon lying in the near infrared region of the electromagnetic spectrum. The plasmon energy is given by $\hbar\omega_p$ where

TABLE I. Binding energies and full widths at half-maximum.

			Binding energy (eV)	Shift relative to SnO ₂ (eV)	FWHM (eV)	Relative area
VB	Undoped SnO ₂	Peak x	4.95			
		Peak y	7.46			
		Peak z	11.07			
	3% Sb-doped SnO ₂	Peak x	5.43	+0.48		
		Peak y	7.96	+0.50		
		Peak z	11.52	+0.45		
Sn 3d _{5/2}	Undoped SnO ₂		487.00		1.04	1.00
	3% Sb-doped SnO ₂	Screened	486.96	-0.04	0.71	0.25
		Unscreened	487.61	+0.61	1.26	0.75
		Baricenter	487.44	+0.44		
Sn 4d _{5/2}	Undoped SnO ₂		26.28		1.10	1.00
	3% Sb-doped SnO ₂	Screened	26.31	+0.03	0.78	0.28
		Unscreened	26.94	+0.66	1.31	0.72
		Baricenter	26.76	+0.48		
O 1s	Undoped SnO ₂		530.87		1.74	1.00
	3% Sb-doped SnO ₂	Screened	531.04	+0.17	0.90	0.52
		Unscreened	531.63	+0.76	1.32	0.48
		Baricenter	531.32	+0.45		

$$\omega_p^2 = \frac{Ne^2}{m^* \epsilon_0 \epsilon(\infty)}. \quad (1)$$

At low beam energies in electron energy-loss spectroscopy the loss probability is dominated by surface scattering, the surface plasmon frequency being given by

$$\omega_p^2 = \frac{Ne^2}{m^* \epsilon_0 [\epsilon(\infty) + 1]}. \quad (2)$$

In both these equations N is the concentration of conduction electrons, e the electronic charge, $\epsilon(\infty)$ the high-frequency dielectric constant, m^* the effective mass of conduction electrons at the Fermi level, and ϵ_0 the permittivity of free space. The effective mass relevant to EELS depends on the dispersion of energy with wave vector k_F at E_F ,

$$\left| \frac{dE}{dk} \right|_{E=E_F} = \left(\frac{h}{2\pi} \right)^2 \frac{k_F}{m^*}. \quad (3)$$

The conduction band in SnO₂ is not strictly parabolic and m^* increases slightly with increasing occupation of the conduction band. Published values of m^* at different doping levels^{6,24} have been fitted to a simple expression of the sort

$$m^* = m_0^* + cN, \quad (4)$$

where m_0^* is the effective mass at the bottom of the conduction band and c is a constant. This fit gives $m^*/m_0 = 0.192$ and $c/m_0 = 0.0259 \times 10^{-20} \text{ cm}^3$.

The surface plasmon energy for the sample of 3% Sb-doped SnO₂ used in the present experiments was measured to be 0.59 eV using excitation with a 100-eV electron beam.²⁶ This corresponds to a carrier concentration of 3.5×10^{20}

cm^{-3} . The concentration of Sb atoms is $8.4 \times 10^{20} \text{ cm}^{-3}$ so that just under one half of the Sb ions act as donor centers. This is due to incorporation of Sb(III) at external and grain boundary surfaces. These ions trap an electron pair but do not act as donor centers.^{16,24}

Since the effective mass shows a linear variation with carrier concentration, the Fermi energy E_F relative to the bottom of the conduction band is given by the integral

$$E_F = \int_0^N \frac{h^2}{4(3\pi^2 n)^{1/3}(m_0^* + cn)} dn. \quad (5)$$

Here N and m^* have the same meanings as in Eq. (1). A standard analytical solution exists for this integral of the form

$$E_F = \frac{a^2}{m_0^*} \left(\frac{h}{2\pi} \right)^2 \left[\frac{1}{6} \ln \frac{X^2 - aX + a^2}{(X+a)^2} + \frac{1}{\sqrt{3}} \times \tan^{-1} \frac{2X-a}{\sqrt{3}a} + \frac{\pi}{6} \right], \quad (6)$$

where

$$X = (3\pi^2 N)^{1/3} \quad (7)$$

and

$$a = \left(\frac{3\pi^2 m_0^*}{c} \right)^{1/3}. \quad (8)$$

Through application of Eq. (6) the width of the occupied part of the conduction band is estimated to be 0.81 eV. This

may be compared directly with a previously published UV photoemission spectrum of 3% Sb-doped SnO_2 ceramic excited at $h\nu = 21.2$ eV.^{15,16} In the earlier work the Sn $5s$ conduction band was compared to a free-electron profile. A fixed effective mass ratio $m^*/m_0 = 0.8$ was derived from a measured surface plasmon energy of 0.55 eV, assuming that all Sb ions act as donor centers and that the conduction band was strictly parabolic. The Sn $5s$ bandwidth derived in this way was just under 0.50 eV. This value was clearly much smaller than an observed bandwidth of approximately 0.75 eV, although the reasons for the discrepancy were not evident at that time. The earlier experimental data are in much better accord with the current estimate of 0.81 eV for the Sn $5s$ bandwidth.

Clearly the shift of valence-band features (0.45 eV) is significantly less than expected from the width of the occupied part of the conduction band. This effect is attributed to shrinkage or renormalization of the bulk band gap with doping. Two effects operate to produce the shrinkage. First, the attractive Coulomb potential associated with the greater nuclear charge of the dopant Sb atoms as compared with the host Sn cations gives rise to an attractive dopant-electron interaction. Second, the conduction electrons act to screen the repulsive conduction-electron–valence-electron Coulomb interaction, thus stabilizing the conduction-band states. The band-gap renormalization of approximately 0.36 eV is of the order of magnitude expected from calculation on Sn-doped In_2O_3 (Ref. 5) using Heine-Abarenkov pseudopotentials to deal with the electron-impurity interactions and the random phase approximation to account for electron-electron interactions. In this work it was found that at a carrier concentration of $4 \times 10^{20} \text{ cm}^{-3}$, the contribution to the band-gap narrowing from electron-impurity and electron-electron interactions were approximately 0.05 and 0.2 eV, respectively.

B. Sn core-level spectra

High-resolution Sn $3d_{5/2}$ core level spectra of undoped SnO_2 and 3% Sb-doped SnO_2 are shown in Fig. 2. Undoped SnO_2 displays a symmetric Voigt profile with a full width at half-maximum (FWHM) height of 1.04 eV. By contrast the spectrum for 3% Sb-doped SnO_2 is much broader with a FWHM of 1.49 eV. The peak shows a well-defined shoulder on the high binding energy side. There is also a small shift of 0.10 ± 0.05 eV to high binding energy in the peak maximum as compared with the undoped material. The shift in the core-level peak is very much less than the shift of valence-band features. Similar effects are observed in the Sn $4d$ region. For the undoped material [Fig. 3(a)], the $4d$ core peak can be fitted to a pair of Voigt profiles constrained to a 3:2 intensity ratio, with an additional weak contribution from the O $2s$ level. Doping produces striking broadening on the high binding energy side of the peaks, again with a small shift to high binding energy in the $4d_{5/2}$ peak maximum [Fig. 3(b)].

The effects of doping can be understood in terms of a screening response of the conduction electron gas introduced by doping in Sb-doped SnO_2 . We can develop a simple heuristic for the core lineshape by assuming that the Koopmans' state in which a core electron is simply removed from the initial state is projected onto "screened" and "unscreened" final eigenstates. A fit of the asymmetric core lines to two

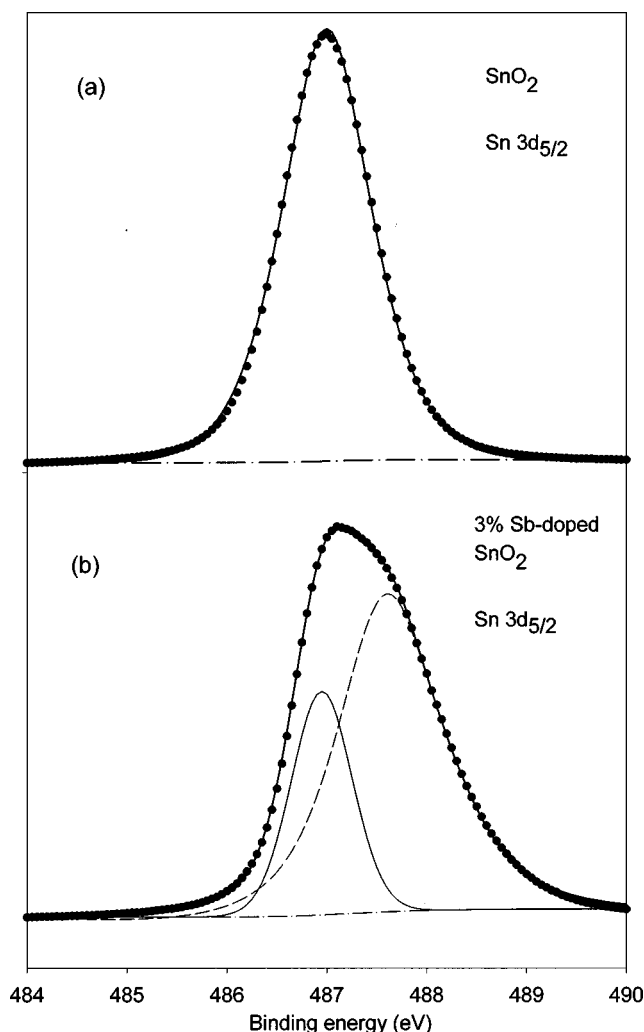


FIG. 2. (a) Sn $3d_{5/2}$ core-level XPS for undoped SnO_2 (filled circles) fitted to a Shirley background (dash-dot line) and a single Voigt function (light solid line). The fit (bold solid line) is seen to pass through the experimental data points. (b) Sn $3d_{5/2}$ core-level XPS for 3% Sb-doped SnO_2 (filled circles) fitted to a Shirley background (dash-dot line) and Voigt profiles for screened (light solid line) and unscreened (dashed line) final states. The fit (bold solid line) is seen to pass through the experimental data points.

Voigt components gives an excellent description of the overall core line shape, as is evident from Figs. 2(b) and 3(b). The low binding energy screened final state carries approximately 25% of the spectral weight in the Sn $3d$ region and 28% in the Sn $4d$ region. The screened state is represented by a Voigt profile whose peak maximum is close to that found for the undoped material. The energy separation between the screened and unscreened final states was found to be 0.65 ± 0.05 eV in the $3d$ region and 0.63 ± 0.05 eV in the $4d$ region. These values are between the bulk and surface plasmon energies of 0.66 and 0.59 eV, respectively. This suggests that the dominant screening response of the electron gas in 3% Sb-doped SnO_2 lies in collective electron excitation. This accords with simple models of intrinsic plasmon excitation in core photoemission of metallic materials. Following Langreth²⁷ and Wertheim,⁹ we can expect the ratio β between a primary photoemission peak and the intrinsic plasmon satellite to be determined by the average separation between conduction electrons r_s ,

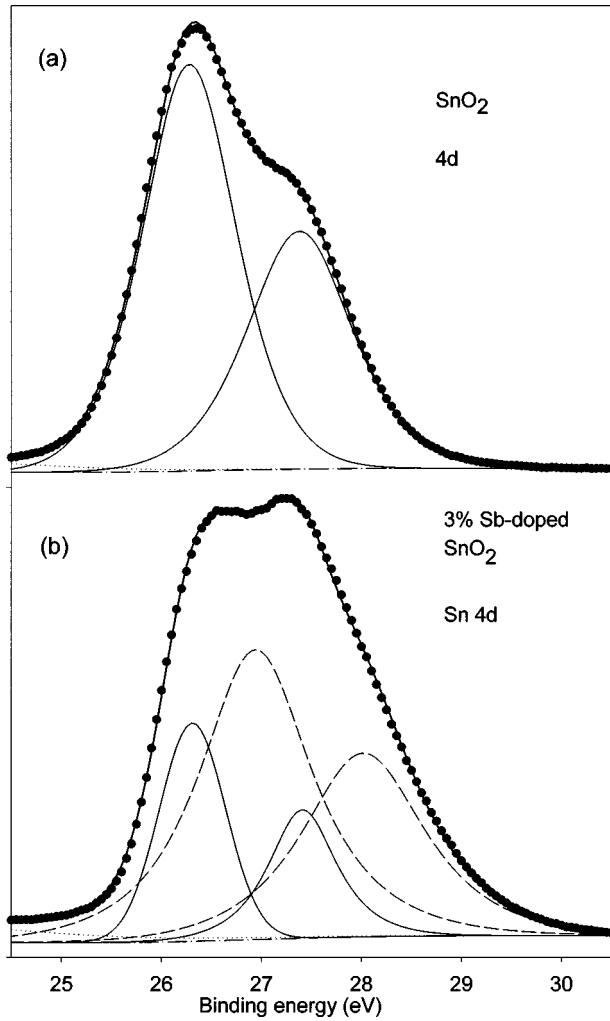


FIG. 3. (a) Sn 4d core-level XPS for undoped SnO_2 (filled circles) fitted to a Shirley background (dash-dot line) and a pair of Voigt functions for $4d_{5/2,3/2}$ components (light solid lines). There is an additional contribution due to the tail from the O 2s peak (dotted line). The fit (bold solid line) is seen to pass through the experimental data points. (b) Sn 4d core-level XPS for 3% Sb-doped SnO_2 (filled circles) fitted to a Shirley background (dash-dot line) and two pairs of Voigt profiles for screened (light solid lines) and unscreened (dashed line) final states. There is an additional contribution due to the tail from the O 2s peak (dotted line). The fit (bold solid line) is seen to pass through the experimental data points.

$$\beta \approx \frac{1}{6} \frac{r_s}{a_0} = \frac{1}{6} \left(\frac{3}{4\pi N} \right)^{1/3} \frac{1}{a_0}, \quad (9)$$

where N is again the carrier concentration and a_0 is the Bohr radius. The electron gas in 3% Sb-doped SnO_2 is very dilute with $r_s/a_0 = 16.6$ so that strong excitation of intrinsic plasmons is expected with $\beta = 2.77$. This is very close to the values observed for the Sn core lines. The agreement must be fortuitous because the simple model of plasmon excitation breaks down in the strong coupling regime where $\beta > 1$. Moreover, the intrinsic plasmon model requires strong excitation of multiple plasmon modes. In addition there must be an extrinsic contribution to the plasmon loss intensity. Empirically we found that the fit to the experimental lineshape could accommodate loss peaks at $2\hbar\omega_p$, but the fit was no

better this new component was introduced. This is not necessarily an observation of physical significance in view of the strong overlap of the primary and plasmon loss peaks. Similarly, the actual fit to the core line profile was not significantly improved by introduction of distinct bulk and surface plasmon peaks.

Our current observations are broadly in line with core photoemission studies of the Na_xWO_3 bronzes,⁹ where strong satellite lines on the W 4f core peaks were interpreted in term of excitation of “local” plasmon modes, the energies of which should lie between those of bulk and surface modes.²⁸ In this earlier work it was also found that screening response involved excitation of a only single plasmon mode. However, in addition it was also observed that the core line associated with the screened final state showed the effects of asymmetric broadening due to single-particle electron-hole pair excitations. The very low energy of the plasmon mode in relation to the overall peak width in the present work precludes any attempt to extract information about possible asymmetry in the core line associated with the screened final state.

Two features of the fits do however deserve further comment. First, it is found that the peak baricenters in 3%-doped SnO_2 , defined by weighting the screened and unscreened peaks by their relative areas, show essentially the same shifts relative to undoped SnO_2 as found in the valence-band spectra. This provides support for the introduction of a Koopmans’ state showing the same initial state shift relative to undoped SnO_2 as the valence-band states.

Second, it is found that the component associated with the screened final state is very much narrower than the peak found for undoped SnO_2 . This can be understood in terms of a significant contribution to the peak width for the undoped material deriving from phonon excitation.²⁹ When an Sn core level is ionized, the surrounding octahedron of O ions finds itself at a distance from the Sn ions that is greater than the new equilibrium distance. Lattice relaxation therefore takes place, but on a time scale longer than that of the photoemission process. The corresponding relaxation energy is given (in atomic units) by

$$E_R = e^2 \left(\frac{6}{\pi V} \right)^{1/3} \left(\frac{1}{\epsilon(\infty)} - \frac{1}{\epsilon(0)} \right), \quad (10)$$

where $\epsilon(\infty)$ and $\epsilon(0)$ are the high- and low-frequency dielectric constants and V is the volume per Sn ion, i.e., half the volume of the tetragonal unit cell. Taking the ϵ values to be the average of values parallel and perpendicular to the c axis:

$$\epsilon = \frac{2}{3} \epsilon_{\perp} + \frac{1}{3} \epsilon_{\parallel} \quad (11)$$

we derive a value $E_R = 0.94$ eV. The relaxation leads to excitation of phonons over a range of energies, giving a Gaussian contribution to the linewidth ΔE_{ph} where

$$\Delta E_{\text{ph}} = 2.35 \left(\hbar \omega_{\text{LO}} E_R \coth \frac{\hbar \omega_{\text{LO}}}{2kT} \right)^{1/2}. \quad (12)$$

Here all of the energy terms including the room-temperature thermal energy kT and the effective longitudinal phonon frequency $\hbar \omega_{\text{LO}}$ are in eV. We take $\hbar \omega_{\text{LO}}$ to be the average of the highest-frequency modes parallel (A_{2u}) and perpendicu-

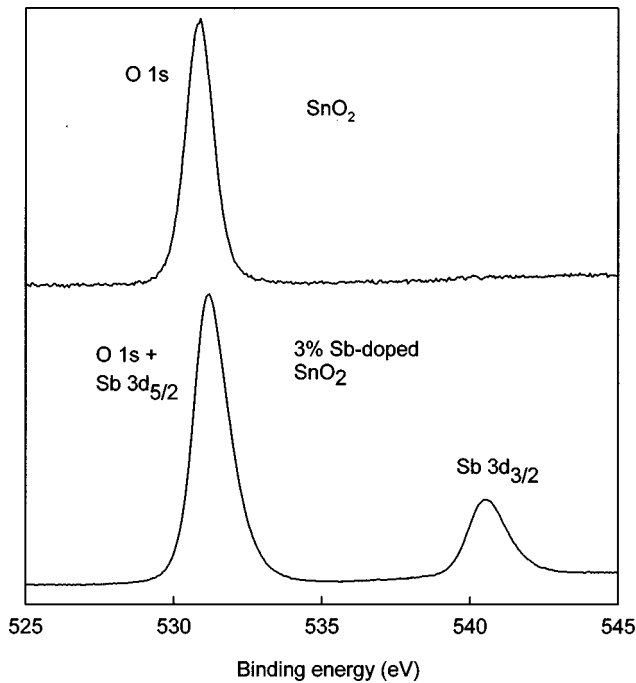


FIG. 4. (a) O 1s spectrum of undoped SnO₂. (b) O 1s plus Sb 3d spectrum of 3% Sb-doped SnO₂. The Sb 3d_{5/2} peak overlaps the O 1s peak almost perfectly in the latter.

lar (E_u) to the c axis. In this way the phonon broadening is estimated to be 0.71 eV. Assuming that this contribution to the overall linewidth adds in quadrature to instrumental and lifetime broadening, we can estimate that, for undoped SnO₂, the nonphonon broadened linewidth is given by ΔE_i where

$$\Delta E_i = (\Delta E_{\text{obs}}^2 - \Delta E_{\text{ph}}^2)^{1/2}. \quad (13)$$

For the Sn 3d_{5/2} line we estimate that $\Delta E_i = 0.76$ eV. This is very close to the value observed for the screened component of the Sn 3d_{5/2} line in 3% Sb-doped SnO₂. Thus it appears that the conduction electrons in the doped material screen out coupling between the Sn core photohole and the phonons. Since the unscreened state involves excitation of bulk and surface plasmons, the overall linewidth of this component depends on the plasmon lifetime and is very much greater than for the screened final state.

C. O 1s core-level spectra

The effects of Sb doping on the O 1s core line are complicated by the fact that the Sb 3d_{5/2} core line shows almost perfect overlap with the O 1s core line (Fig. 4). The intensity of the Sb core-level peaks is very much greater than expected from the bulk doping level. This is attributed to segregation of Sb(III) to surface sites where Sn(II) is replaced, as discussed earlier. Prior to analysis of the O 1s core line it was therefore necessary to strip the composite O 1s + Sb 3d_{5/2} peak of structure due to the Sb core level. This was achieved by multiplying the Sb 3d_{5/2} peak by $\frac{3}{2}$, shifting to low binding energy by the measured spin-orbit coupling constant for Sb (9.37 eV) (Ref. 30) and subtracting this intensity from the composite peak. The resulting O 1s peak profile is shown in Fig. 5. For undoped SnO₂ the O 1s core line can be fitted by a single Voigt function [Fig. 5(a)]. Doping again gives rise to

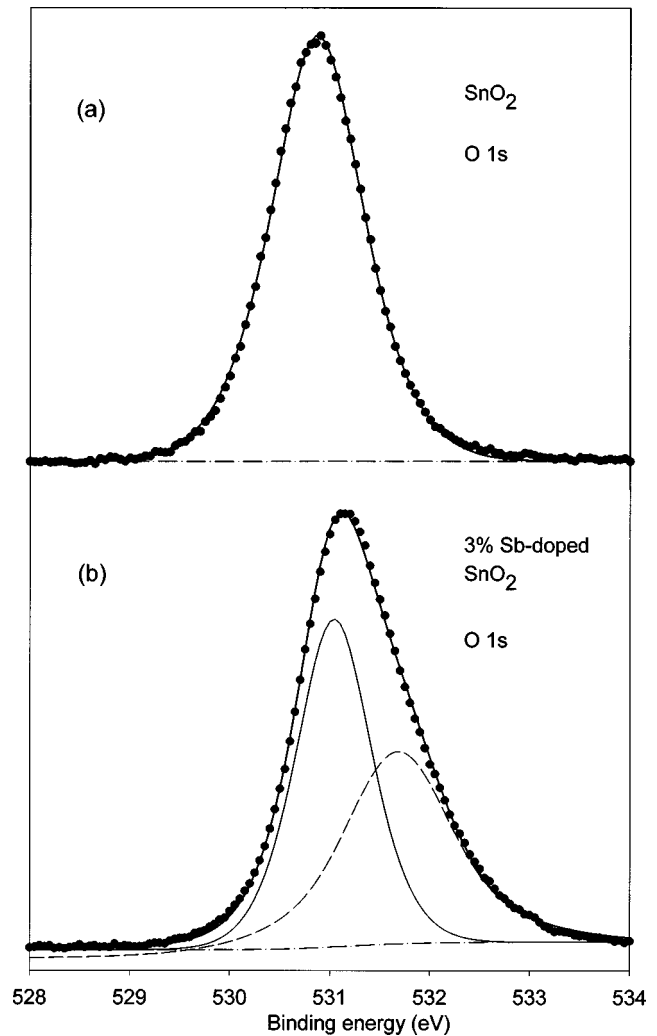


FIG. 5. (a) O 1s core line XPS for undoped SnO₂ (filled circles) fitted to a Shirley background (dash-dot line) and a single Voigt function (light solid line). The fit (bold solid line) is seen to pass through the experimental data points. (b) O 1s core-level XPS for 3% Sb-doped SnO₂ (filled circles) fitted to a Shirley background (dash-dot line) and Voigt profiles for screened (light solid line) and unscreened (dashed line) final states. The fit (bold solid line) is seen to pass through the experimental data points.

line broadening on the high binding energy side [Fig. 5(b)], but this is much less pronounced than for the Sn core lines. Again fitting the overall peak to screened and unscreened components gives a satisfactory heuristic fit to the spectral profile. It is found that the screened final state is more strongly shifted to high binding energy than for the Sn core lines. This implies that the final state screening of the O 1s core hole is much less pronounced than the screening of the Sn core holes. This shows that the screening response of the conduction electron gas is indeed very local in character and is influenced by the fact that the conduction band states are of dominant Sn 5s atomic character. In accordance with this idea, the probability of plasmon excitation is much less for the O 1s core level than for the Sn core levels. However, as for the Sn core lines, the baricenter of the O 1s spectral weight shows roughly the same shift (0.45 eV) relative to the O 1s binding energy of the undoped material as is found in the valence-band region (0.40 eV). The pronounced differ-

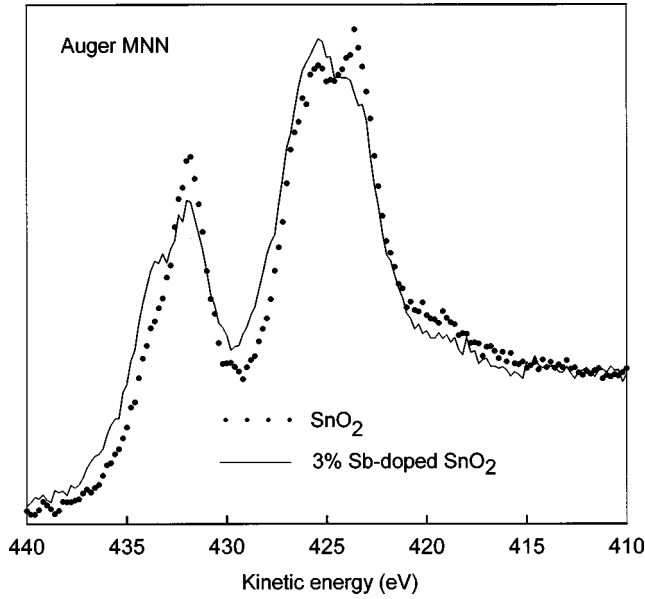


FIG. 6. *MNN* Auger spectra for undoped SnO_2 (dotted) and 3% Sb-doped SnO_2 (solid line).

ences in the contribution of plasmon loss structure to O 1s and Sn 3d line shapes reinforces the view that the plasmon loss intensity is not dominantly extrinsic in the 3d region.

D. Auger spectra

MNN Auger spectra for SnO_2 and 3% Sb-doped SnO_2 are shown in Fig. 6. Doping is seen to produce a pronounced shift in spectral weight to high kinetic energy. This can be understood in terms of Auger structure associated with screened Sn 3d and 4d core holes. As we have seen, final-state screening stabilizes one Sn 3d core hole state, thus producing a downward contribution to the binding energy shift that competes with the initial-state shift associated with conduction-band filling. The total binding energy shift for the screened final state may be written as $\Delta E_B(3d)$ where³¹

$$\Delta E_B(3d) = -\Delta\epsilon(3d) - \Delta R^{\text{ea}}(3d); \quad (14)$$

here $\epsilon(3d)$ is the initial state 3d orbital energy and $R^{\text{ea}}(3d)$ is the extra-atomic relaxation energy associated with screening of a 3d core hole. This expression assumes that the intra-atomic relaxation energy is unaffected by doping. The delocalized holes in the O 2p valence-band states must experience a much smaller screening response from the Sn 5s conduction electrons than the localized Sn 3d or 4d core holes. This screening energy may be taken to define a zero reference point for other screening energies. If we assume that all states suffer the same rigid initial-state shift due to doping, $\Delta R^{\text{ea}}(3d)$ may be estimated as the difference between the mean shift in valence-band features due to doping (+0.45 eV) and the 3d shift (−0.04 eV), i.e., 0.49 eV. Likewise the relaxation energy shift for the Sn 4d core hole is 0.45−0.03 eV=0.42 eV. Thus the screening for the more delocalized 4d core hole is slightly less than for the 3d core hole.

The shift in kinetic energy for $M_4N_{4,5}N_{4,5}$ Auger electrons is given by $\Delta E_K(3d,4d,4d)$, where

$$\Delta E_K(3d,4d,4d) = 2\Delta\epsilon(4d) - \Delta\epsilon(3d) - \Delta R^{\text{ea}}(3d) + \Delta R^{\text{ea}}(4d,4d), \quad (15)$$

where $\Delta R^{\text{ea}}(4d,4d)$ is the change in extra-atomic relaxation associated with the Auger final state with two holes in the 4d shell. With the usual assumption that the screening energy for a two-hole state is four times that of a one-hole state and that $\Delta\epsilon(4d) = \Delta\epsilon(3d) = \Delta\epsilon$ we have³¹

$$\Delta E_K(3d,4d,4d) = \Delta\epsilon - \Delta R^{\text{ea}}(3d) + 4\Delta R^{\text{ea}}(4d). \quad (16)$$

Thus Auger structure associated with screened final states shifted by $[-0.45 - 0.49 + 4(0.42)] = 0.74$ eV to high kinetic energy of the structure found for undoped SnO_2 is expected upon doping. The *MNN* Auger spectra are shown in Fig. 6. The large width of the Auger features and the complex peak shapes preclude any simple fitting procedure and make it difficult to establish the magnitude of the upward shift in kinetic energy. However, it is quite clear that doping leads to a shift in spectral weight to high kinetic energy, as required by our simple analysis. Thus Auger spectroscopy confirms the important role of final state screening effects in core photoemission from Sb-doped SnO_2 .

IV. CONCLUDING REMARKS

3% Sb doping in SnO_2 produces pronounced changes in valence- and core-level photoemission spectra. Valence-band features show a simple shift to high binding energy with doping, although this is smaller than the width of the occupied part of the conduction band. The difference between conduction-band width and the observed shift provides a direct way of probing band-gap shrinkage arising from the *n*-type doping: previous investigations of this effect in oxide systems^{4–6} have relied on optical measurements, which in themselves are unable to unravel the competing influences of valence- and conduction-band dispersion and band-gap renormalization on shifts in optical absorption edges.

The effects of doping on core-level spectra are more complicated. Pronounced changes in core line shapes indicate the presence of discrete screened and unscreened final states in the doped material. The baricenters of these two states show the same shifts with doping as found in the valence region. The dominant screening mechanism involves excitation of conduction electron plasmons. The response of the electron gas to core ionization is broadly similar to that found for materials such as the sodium tungsten bronzes,⁹ although in the present case we are dealing with a very much more dilute electron system than has been previously studied earlier. Further theoretical work is needed to clarify the mechanisms that lead to coupling between the core photohole and the carriers in degenerately doped oxide semiconductors of the sort studied in the present work.

ACKNOWLEDGMENTS

J.R. is grateful to the Soros Foundation for financial support. We thank Dr. G. Beamson and Mr. D. Kinder for technical assistance.

- * Author for correspondence. Electronic address: russ.egdell@chem.ox.ac.uk
- [†] On leave from Department of Inorganic Chemistry, Moscow State University, Russia.
- ¹ D. Fröhlich, R. Klenkies, and R. Helbig, *Phys. Rev. Lett.* **41**, 1750 (1978).
- ² H. Köstlin, *Festkörperprobleme* **XXII**, 229 (1982).
- ³ K. F. Bergren and B. E. Sernelius, *Phys. Rev. B* **24**, 1971 (1981).
- ⁴ Z. C. Jin, I. Hamberg, C. G. Granquist, B. E. Sernelius, and K. F. Bergren, *Thin Solid Films* **164**, 381 (1988).
- ⁵ I. Hamberg, K. F. Bergren, L. Engstrom, C. G. Granquist, and B. E. Sernelius, *Phys. Rev. B* **30**, 3240 (1984).
- ⁶ G. Sanon, R. Rup, and A. Mansingh, *Phys. Rev. B* **44**, 5672 (1991).
- ⁷ E. Burstein, *Phys. Rev.* **93**, 632 (1954).
- ⁸ Y. Dou, T. Fishlock, R. G. Egdell, D. S. L. Law, and G. Beamson, *Phys. Rev. B* **55**, R13 381 (1997).
- ⁹ J. N. Chalzalviel, M. Campagna, and G. K. Wertheim, *Phys. Rev. B* **16**, 697 (1977).
- ¹⁰ H. Höchst, R. D. Bringans and H. R. Shanks, *Solid State Commun.* **37**, 41 (1980).
- ¹¹ G. K. Wertheim and J. N. Chalzalviel, *Solid State Commun.* **40**, 931 (1981).
- ¹² J. W. Allen, C. G. Olson, M. B. Maple, J.-S. Kang, L. Z. Liu, J.-H. Park, R. O. Anderson, W. P. Ellis, J. T. Markert, Y. Dali-chauouch, and R. Liu, *Phys. Rev. Lett.* **64**, 595 (1990).
- ¹³ Z.-X. Shen, D. S. Dessau, B. O. Wells, C. G. Olson, D. B. Mitzi, L. Lombardo, R. S. List, and A. J. Arko, *Phys. Rev. B* **44**, 12 098 (1991).
- ¹⁴ T. R. Cummins and R. G. Egdell, *Phys. Rev. B* **48**, 6556 (1993).
- ¹⁵ P. A. Cox, R. G. Egdell, C. Harding, A. F. Orchard, W. R. Patterson, and P. J. Tavener, *Solid State Commun.* **44**, 837 (1982).
- ¹⁶ P. A. Cox, R. G. Egdell, C. Harding, W. R. Patterson, and P. J. Tavener, *Surf. Sci.* **123**, 179 (1982).
- ¹⁷ R. G. Egdell, W. R. Flavell, and P. J. Tavener, *J. Solid State Chem.* **51**, 345 (1984).
- ¹⁸ C. Lau and G. K. Wertheim, *J. Vac. Sci. Technol.* **15**, 622 (1978).
- ¹⁹ J. M. Themlin, M. Chtaib, L. Henrard, P. Lambin, J. Darville, and J. M. Gilles, *Phys. Rev. B* **46**, 2460 (1992).
- ²⁰ L. Kover, Z. Kovacs, R. Sanjines, G. Moretti, I. Cserny, G. Margaritondo, J. Palinkas, and H. Adachi, *Surf. Interface Anal.* **23**, 461 (1995).
- ²¹ R. G. Egdell, S. Eriksen and W. R. Flavell, *Solid State Commun.* **60**, 835 (1986).
- ²² D. F. Cox, T. B. Fryberger, and S. Semancik, *Phys. Rev. B* **38**, 2072 (1988).
- ²³ J. M. Themlin, R. Sporken, J. Darville, R. Caudano, J. M. Gilles, and R. L. Johnson, *Phys. Rev. B* **42**, 11 914 (1990).
- ²⁴ R. G. Egdell, in *Science of Ceramic Interfaces II*, edited by J. Nowotny (Elsevier, Amsterdam, 1994), p. 527.
- ²⁵ I. Manassidis, J. Goniakowski, L. N. Kantorovitch, and M. J. Gillan, *Surf. Sci.* **339**, 258 (1995).
- ²⁶ At 100 eV exciting energy, the total plasmon loss intensity is very close to that expected from the dielectric model of surface scattering. See, for example, H. Ibach and D. L. Mills, *Electron Energy Loss Spectroscopy and Surface Vibrations* (Academic, New York, 1982) for a discussion of surface dipole scattering.
- ²⁷ D. C. Langreth, *Phys. Rev. Lett.* **26**, 1229 (1971).
- ²⁸ E. A. Sziklas, *Phys. Rev. B* **138**, A1070 (1965).
- ²⁹ M. Iwan and C. Kunz, *Phys. Lett.* **60A**, 345 (1977).
- ³⁰ R. Nyholm and N. Martensson, *Solid State Commun.* **40**, 311 (1981).
- ³¹ S. D. Waddington, in *Practical Surface Analysis*, edited by D. Briggs and M. P. Seah (Wiley, Chichester, 1994), p. 587.